

# Phosphorus speciation in calcite speleothems determined from solid-state NMR spectroscopy

Harris E. Mason<sup>a</sup>, Silvia Frisia<sup>b</sup>, Yuanzhi Tang<sup>a</sup>,  
Richard J. Reeder<sup>a</sup>, Brian L. Phillips<sup>a,\*</sup>

<sup>a</sup> Center for Environmental Molecular Science, Department of Geosciences,  
State University of New York, Stony Brook, New York, 11794-2100, United States

<sup>b</sup> Museo Tridentino di Scienze Naturali, via Calepina 14, 38100 Trento, Italy

Received 27 June 2006; received in revised form 9 November 2006; accepted 25 November 2006

Available online 10 January 2007

Editor: H. Elderfield

## Abstract

Variations in speleothem P concentration show cyclic patterns that have important implications for high resolution palaeoclimate and palaeoenvironmental reconstructions. However, little is known about the speciation of P in calcite speleothems. Here we employ solid-state <sup>31</sup>P and <sup>1</sup>H magic angle spinning nuclear magnetic resonance (MAS NMR) spectroscopic techniques as a non-destructive method for analyzing the distribution of P in speleothems. The <sup>31</sup>P MAS NMR results show three peaks indicating the presence of three primary types of phosphate species in samples from the Grotta di Ernesto (northeastern Italy): a broad peak at a chemical shift  $\delta_{P-31}=3.1$  to 3.7 ppm from individual phosphate ions incorporated within calcite, a narrow set of peaks near  $\delta_{P-31}=-0.9$  ppm from crystalline monetite and a narrow peak at  $\delta_{P-31}=2.9$  ppm from an unidentified crystalline phosphate phase. Essentially identical results were obtained for a synthetic calcite/phosphate coprecipitate. Spectra collected for a sample from Grotte de Clamouse (southern France) show only a broad peak near 3.5 ppm suggesting a possible limit for phosphate incorporation into the calcite structure. These data suggest that P in this system can interact to form calcium phosphate surface precipitates during infiltration events and are subsequently enclosed during calcite growth.

© 2006 Elsevier B.V. All rights reserved.

**Keywords:** speleothem; phosphate; calcite; NMR spectroscopy

## 1. Introduction

Speleothems are becoming one of the most promising archives of high resolution climate and environmental proxy data in a variety of continental settings. The last 5 years has seen a rapid advance in techniques capable of analyzing trace element concentrations in

speleothem calcite at very high spatial resolution. The corresponding time series of trace element variability in stalagmites and stalactites are of great palaeoenvironmental and palaeoclimate significance. Furthermore, chemical time series can provide annual chronological markers [1]. The application of secondary ionization mass spectrometry (SIMS) [2–5] and excimer, laser-ablation inductively coupled plasma mass spectrometry (ELA-ICPMS) [6,7] has allowed rapid generation of scans at a spatial resolution of the order of 10  $\mu$ m. In

\* Corresponding author. Tel.: +1 631 632 6853; fax: +1 631 632 6840.  
E-mail address: [brian.phillips@sunysb.edu](mailto:brian.phillips@sunysb.edu) (B.L. Phillips).

these studies, P and Mg concentrations exhibit clear cycles which have been related to hydrology [6], temperature, and prior calcite precipitation [3].

In annually laminated specimens from Grotta di Ernesto, the association of high P content with visible, ca. 0.5 to 4  $\mu\text{m}$ -thick, dark layers capping each lamina, has been interpreted as recording a short period of increased P supply during autumnal infiltration events [4]. Phosphorus appears, therefore, to be one of the trace elements that most clearly defines annual cycles in speleothems; its distribution appears to be related to the pattern of annual layering in a variety of environmental settings [4,6]. Little is known, however, about the form in which P is present within cave calcite. The P-rich dark laminae fluoresce, implying that they contain higher concentrations of organic compounds derived from the soil zone [8]. P could be associated with a soil-derived organic fraction brought into the cave during the autumn rains. However, on the basis of average C/P ratio in soil organic matter, Huang et al. estimated that organic P in stalagmites from Grotta di Ernesto should amount to a maximum of ca. 9 ppm [4], which is much lower than the average of 43 ppm measured by SIMS. Huang et al., therefore, infer that the bulk of P is inorganic, but considered the distribution pattern to be inconsistent with submicroscopic apatite grains because P commonly encompasses the inclusion-rich layer. The current interpretation is that at concentrations below 100 ppm P may be present in speleothems as individual phosphate ions incorporated within the calcite structure [4], which reflects cave hydrology, and water chemistry variability [9].

Synchrotron radiation generated micro XRF maps at 2  $\mu\text{m}$  resolution have shown that the lateral distribution of P in the annually laminated speleothems from Grotta di Ernesto follows laterally the visible dark layers marking each lamina. The range of P concentration within each dark layer is, however, wide [9]. Micrometer to sub-micrometer sized P-rich pixels may be interpreted as associated with submicroscopic grains, which, if the hypothesis of Huang et al. [4] is correct, may not be apatite but some other phase or P adsorbed on colloidal particles [10]. Micrometer-sized, C-rich particles have indeed been observed by scanning electron microscopy in association with the calcite surface which grew across the autumnal flushing at Grotta di Ernesto [11].

Interactions between calcite and dissolved P have been studied extensively due to the potential role of phosphate in the inhibition of calcite crystal growth and the importance of phosphate sorption to mineral surfaces for mediating the geochemical cycling of P [12–20].

House and Donaldson [16] investigated phosphate adsorption and coprecipitation over a pH range of 7 to 9.5 using P concentrations of 1 to 18  $\mu\text{mol L}^{-1}$  and calcite with a surface area of 0.22 and 0.37  $\text{m}^2 \text{g}^{-1}$ , corresponding to a maximum surface loading of 4.9  $\text{P nm}^{-2}$ . They concluded that phosphate coprecipitation, which gave overgrowths having  $>2000$  ppm P, could be adequately explained by a two component adsorption model of  $\text{PO}_4^{3-}$  or  $\text{CaPO}_4$  and  $\text{HPO}_4^{2-}$  or  $\text{CaHPO}_4$ . In addition they noted that during their adsorption experiments 80% of the P was removed from solution within the first 2 min after addition of calcite to the system. Hinedi et al. [21] used solid-state  $^1\text{H}$  and  $^{31}\text{P}$  NMR spectroscopy to investigate phosphate sorption onto a high surface area calcite (22  $\text{m}^2 \text{g}^{-1}$ ). At phosphate loadings of 0.002 to 1.0  $\text{P nm}^{-2}$  (0.79 to 36.72  $\mu\text{mol P g}^{-1}$  calcite) they observed the sorption of unprotonated phosphate groups, and at higher phosphate loadings of 1.9 to 3.5  $\text{P nm}^{-2}$  (69.92 to 128.22  $\mu\text{mol P g}^{-1}$  calcite) the formation of brushite was observed. Dove and Hochella [22] studied calcite precipitation on a 3  $\text{mm}^3$  calcite crystal in the presence of 6  $\mu\text{mol/L}$  phosphate ( $8.7 \times 10^5 \text{ P nm}^{-2}$ ) with scanning force microscopy and found growth to proceed by the initial formation of unidentified globular surface precipitates followed by jagged step progression. These studies suggest that removal of dissolved P in the presence of calcite can occur quickly and by several processes including sorption, coprecipitation, and formation of surface precipitates.

Clearly, an understanding of the chemical form of P within calcite is needed, otherwise interpretation of climate and environmental proxy data becomes very difficult [10]. For example, it is possible that P concentration variations in calcite may reflect limits of the ability of calcite to incorporate phosphate ions brought about by factors other than the P concentration of the precipitating fluid. Given the broader implications that P in carbonates has as a palaeoenvironmental indicator in a variety of environments [23], the present study aims at understanding its incorporation within natural and synthetic calcite. For this purpose, we used solid-state  $^{31}\text{P}$  nuclear magnetic resonance (NMR) spectroscopy, which can measure the P speciation in natural materials [24–27]. Cave carbonates are good candidates for solid-state NMR spectroscopic studies because they exhibit a low abundance of paramagnetic ions [28]. Results for speleothem calcite from different climatic settings, including the Grotta di Ernesto speleothems for which P-rich layers seem to be good annual markers, and laboratory-grown crystals indicate that P can be incorporated in speleothem calcite through several processes, including coprecipitation and the

formation of surface precipitates of crystalline calcium phosphate phases.

## 2. Materials and methods

For the present study we chose specimens from two caves, Grotta di Ernesto and Grotte de Clamouse, characterized by different environmental, geologic and hydrologic settings, and for which much information is already available [11,29–31]. Speleothems from these caves have been studied for palaeoclimate and environmental reconstruction [29,32].

Grotta di Ernesto is a shallow cave (ca. 20 m below the surface), located at an elevation of 1167 m in northeast Italy. It is cut in dolomitized limestone overlain by brown calcareous soil up to 1.5 m thick supporting a mixed conifer and deciduous wood. Mean annual temperature at the cave site is ca. 6.7 °C and mean annual rainfall ca. 1300 mm/year, which results in positive net infiltration, with maxima between October and November following high rainfalls [11]. The cave hydrology responds to major recharge events in a relatively short time, from a few days up to 3 months [33], which result in the development of visible annual laminae in most Holocene stalagmites. Measured cave water pH values range from 7.9 to 8.5, and the saturation index (as  $\log(IAP/K_{eq})$ ) of the drips from 0.1 to 0.35. Typical P concentrations for the Grotta di Ernesto drip water range from 0.10 to 0.26  $\mu\text{mol L}^{-1}$ , but can range from 0.97 to 1.61  $\mu\text{mol L}^{-1}$  during infiltration events [3]. Annual laminae of the speleothems consist of a thick, translucent and a thin dark layers [11,33]. Modern cave calcite is mostly characterized by a few dislocations. In older portion of the specimens, microstructures such as dislocations and lamellae have been observed when the order in the stacking of the crystals is perturbed with increasing proportion of the dark layer in successive laminae [11].

Grotte de Clamouse is a relatively deep cave, which develops >50 m below the surface cut in partially dolomitized limestone. The present climate is typically Mediterranean, with mean annual temperature of ca. 14.5 °C and mean annual rainfall ca. 750 mm/year. Due to the dry conditions during summer months, negative infiltration is observed in June, July and August. Nevertheless, drips are relatively constant throughout the year; the hydrology of the cave is characterized by a high proportion of storage water in the aquifer. Measured cave water pH values range from ca. 7.6 to ca. 7.8, and the saturation index of the drips ranges from –0.04 to 0.6 [30]. Holocene stalagmites commonly do not show visible or UV-fluorescent annual laminae. At

present there is no information on P content in the drip waters. Previous studies indicate, however, that some trace elements such as Mg and Sr show annual variations [32]. Under the present-day cave environmental conditions, the calcite crystals are translucent, and show no microstructures or a few dislocations [30]. The crystals composing the speleothems from these two caves differ and may potentially reflect different incorporation of P.

The natural samples we analysed consisted of three calcite stalagmite speleothem samples: ER67 (sub-sample a, unpublished), still active when removed, and the Holocene ER77 (subsample L) [33] and ER78 (subsample L) [9] from the Grotta di Ernesto, and the tip of stalagmite CL23 (unpublished), consisting of clearly visible calcite crystals, still active at the time of removal, from Grotte de Clamouse. Bulk samples of the ER67a, ER77.3L and ER78L speleothems were crushed to pass a 120  $\mu\text{m}$  sieve and then bleached for an excess of 9 days in a 6% commercial sodium hypochlorite solution to remove any organic material. Previous work has reported P contents of  $69 \pm 20$  ppm from SIMS traverses for similar speleothems from Grotta di Ernesto [3,4], and concentrations about three times lower for a different sample from Grotte de Clamouse [34].

For phosphate coprecipitation with calcite we used a seeded constant-addition method adapted from Zhong and Mucci [35] and Tesoriero and Pankow [36] as described by Reeder et al. [37]. To a stirred reaction vessel containing 0.7 L of a solution with 0.007 M  $\text{CaCl}_2$  and 0.007 M  $\text{NaHCO}_3$  and a 0.1 M NaCl background electrolyte, 0.5 g of reagent grade calcite from Alfa Aesar (5  $\mu\text{m}$  particle size) was added as nucleation seeds. A solution containing 0.1 M  $\text{CaCl}_2$  and 0.1 M NaCl was pumped through a syringe at a constant rate of 150  $\mu\text{L}/\text{min}$  into the reaction vessel while bubbling continuously with water-saturated air. From a second syringe a solution containing 0.1 M  $\text{Na}_2\text{CO}_3$ , 0.1 M NaCl and 20  $\mu\text{M}$   $\text{K}_2\text{HPO}_4$  was pumped through anti-diffusion tips at the same rate. The total reaction time was 9 h, yielding 1.0 g of phosphate-containing calcite overgrowth on the 0.5 g of seed crystals. The initial solution had a measured pH of 7.86 and was supersaturated with respect to pure calcite, with a saturation index of 1.1 (expressed as  $\log(IAP/K_{eq})$ ), as calculated using the program PHREEQC [38]. During growth the solution pH increased initially and reached a constant value of  $8.25 \pm 0.1$  within 4 to 5 h. Total  $\text{CO}_2$  content in the solution was measured using the procedure described by Hall and Aller [39] and, along with pH, was used to assess when the system had

reached a near steady-state with respect to calcite supersaturation. As the coprecipitation reaction proceeded, the total amount of  $\text{CO}_2$  dropped continuously until near steady-state conditions were achieved, after around 5 h. At near steady-state the saturation index with respect to pure calcite was 0.44, as calculated using the program PHREEQC [38]. The final calcite powder was collected by vacuum filtration, washed multiple times with deionized water, and dried in an oven at 50 °C. X-ray diffraction (XRD) revealed only calcite phase. The total phosphate added to the system during crystal growth corresponds to 52 ppm P in the overgrowths, somewhat lower than the average P concentration for the Grotta di Ernesto samples.

All of the NMR spectra were collected on a 400 MHz Varian Inova spectrometer under magic-angle-spinning (MAS) conditions, at operating frequencies of 161.8 MHz and 399.8 MHz for  $^{31}\text{P}$  and  $^1\text{H}$ , respectively. For the  $^{31}\text{P}$  experiments, samples were contained in 7.5 mm (o.d.)  $\text{Si}_3\text{N}_4$  rotors and spun at 5 kHz. Single-pulse (SP)  $^{31}\text{P}$  spectra were obtained with 3  $\mu\text{s}$  pulses and relaxation delays that varied from 2 to 1000 s. Spectra taken at 500 s relaxation delay were used to obtain relative concentration ratios; spectra taken for some samples at a 1000 s relaxation delay showed no further increase in absolute intensity. For the CP/MAS experiments, contact times of 1–2 ms were used. The probe and rotor assemblies yielded no detectable  $^{31}\text{P}$  NMR signal after several days of acquisition. However, standard  $\text{ZrO}_2$ -based rotor sleeves give  $^{31}\text{P}$  signals in the spectral region for orthophosphate groups. The  $^{31}\text{P}$  NMR chemical shifts ( $\delta_{\text{P-31}}$ ) are referenced with respect to 85% phosphoric acid, using hydroxylapatite as a secondary reference set to  $\delta_{\text{P-31}}=2.65$  ppm. The  $^1\text{H}$  SP MAS NMR spectra were obtained using a Chemagnetics probe assembly configured for 4 mm (o.d.) rotors and modified to yield very low  $^1\text{H}$  background signal. A spinning rate of 15 kHz and a 90° pulse width of 3.5  $\mu\text{s}$  were used. The  $^1\text{H}$  NMR chemical shifts ( $\delta_{\text{H-1}}$ ) are referenced with respect to tetramethylsilane (TMS) using adamantane as a secondary reference set to  $\delta_{\text{H-1}}=2.0$  ppm.

### 3. Results and discussion

The  $^{31}\text{P}$  NMR spectra of all the samples studied can be described by three orthophosphate components consisting of a broad peak with a chemical shift near  $\delta_{\text{P-31}}=3.5$  ppm, a narrow resonance at  $\delta_{\text{P-31}}=2.9$  ppm and a narrow set of peaks centered near  $\delta_{\text{P-31}}=-1$  ppm. The single-pulse (SP) spectra in Fig. 1 show all of the P environments in the samples, but were obtained under

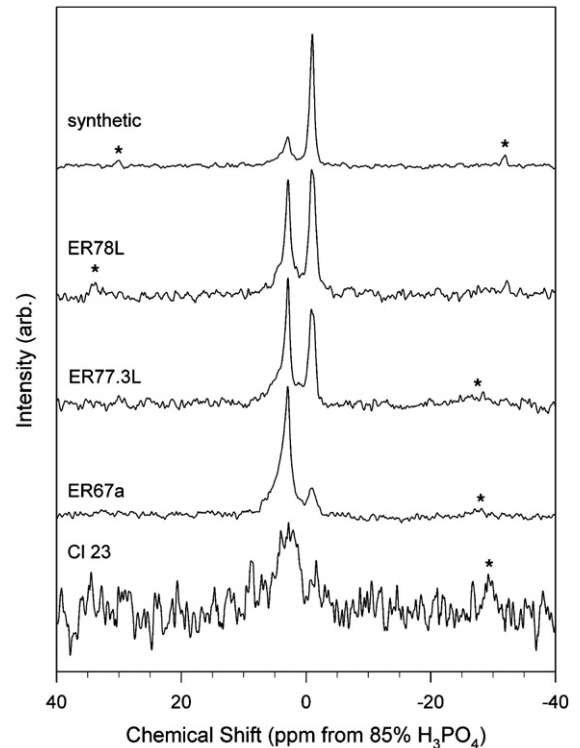


Fig. 1.  $^{31}\text{P}$  single-pulse (SP) MAS NMR spectra of speleothem and synthetic samples studied. Spectra were collected at a spin rate of 5 kHz and a pulse delay of 2 s for (from bottom to top) 42,386, 127,221, 42,272, 42,029, and 45,580 acquisitions. Asterisks denote spinning sidebands.

experimental conditions that suppress the narrow peak at 2.9 ppm so that the broad peak near 3.5 ppm can be distinguished. The intensities of the NMR peaks depend on the  $^{31}\text{P}$  spin-lattice relaxation time and the experimental relaxation delay [40]. The relaxation times differ substantially among the distinct P environments, with that for the peak at  $\delta_{\text{P-31}}=2.9$  ppm being by far the longest. Thus, the relative intensity of the peak at 2.9 ppm appears smaller at short relaxation delay. Fig. 2a shows a typical spectrum (for ER78L) obtained under quantitative conditions, in which the integrated areas of the peaks are proportional to the concentration of the corresponding P environments. The  $^{31}\text{P}\{^1\text{H}\}$  cross-polarization (CP) spectra (Fig. 3) contain signal only for P that is in close spatial proximity to H (less than about 4 Å). The calcite seeds used to prepare the synthetic calcite/phosphate coprecipitate yielded no detectable  $^{31}\text{P}$  NMR signal by SP or CP methods, thus the spectra for this sample correspond only to P in the overgrowths even though NMR detects the entire sample.

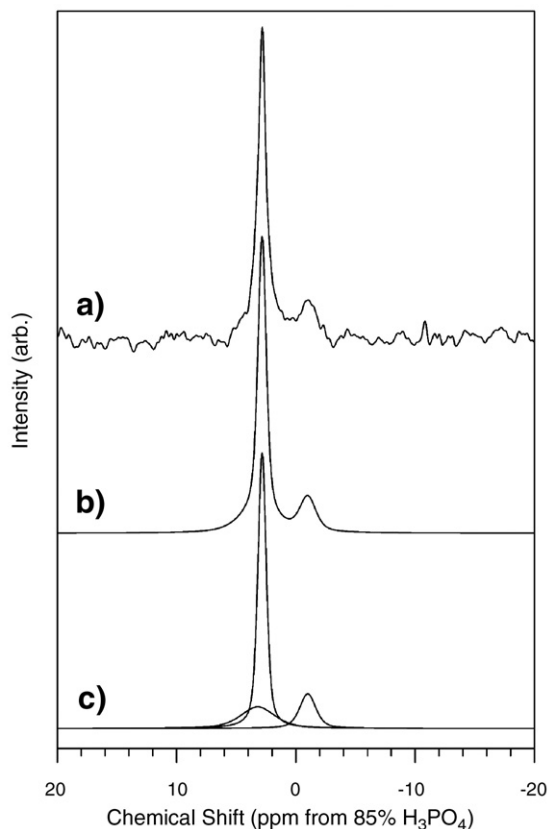


Fig. 2. **a)**  $^{31}\text{P}$  SP MAS NMR spectrum of calcite speleothem ER78L acquired under quantitative conditions, corresponding to 472 acquisitions at a relaxation delay of 500 s. **b)** The spectral profile from a least-squares fit to the experimental data. **c)** The individual curves for the least-squares fit shown in **b)**, corresponding to the principal phosphate environments: phosphate in calcite ( $\delta_{\text{P-31}}=3.2$  ppm, 3.6 ppm FWHM), unidentified crystalline inclusion ( $\delta_{\text{P-31}}=3.0$  ppm, 0.6 ppm FWHM), and monetite ( $\delta_{\text{P-31}}=-1$  ppm, 1.1 ppm FWHM).

All samples show a broad peak at  $\delta_{\text{P-31}}=3.1$  ppm to 3.7 ppm (3.6–3.8 ppm full width at half-maximum; FWHM) in both the SP and CP spectra (Figs. 1 and 3, and Table 1). This peak is similar in position and width to that reported by Hinedi et al. [21], which they assigned to unprotonated phosphate groups sorbed onto the surface of calcite. In our samples this peak likely represents phosphate groups that have sorbed onto the surface and subsequently become incorporated as defects during calcite growth. The large width of this peak indicates a distribution of phosphate environments (e.g., bond lengths and angles), as would be expected for a defect structure. The presence of this peak in CP spectra indicates that it corresponds to P in close proximity to H. It is likely that even if these coprecipitated phosphates are unprotonated, other H-bearing species are likely to be present and serve to

accommodate the charge imbalance and structural defects created by phosphate substitution in the calcite structure. This observation is in agreement with reports of high levels of H detected by ion probe in the dark, autumnal portion of Grotta di Ernesto stalagmite annual laminae, where P concentration also increases [3,4], and with the  $^1\text{H}$  NMR data presented below. The H detected by ion microprobe is consistent with the presence of molecular water or nano-inclusions [41]. However, CP signal requires rigid H species, perhaps indicative of structural defects.

Narrow peaks at a chemical shift near  $\delta_{\text{P-31}}=-0.9$  ppm (1.1 to 1.5 ppm FWHM) occur in both the SP and CP spectra taken for the Grotta di Ernesto samples and the synthetic calcite/phosphate coprecipitate (Figs. 1 and 3, and Table 1). In most spectra this peak occurs at the average position for the two peaks characteristic of crystalline monetite ( $\text{CaHPO}_4$ ) [42,43], which were not resolved in these spectra due to the low  $^1\text{H}$  decoupling power used. The CP spectrum taken for the synthetic sample (Fig. 3) clearly shows two peaks at

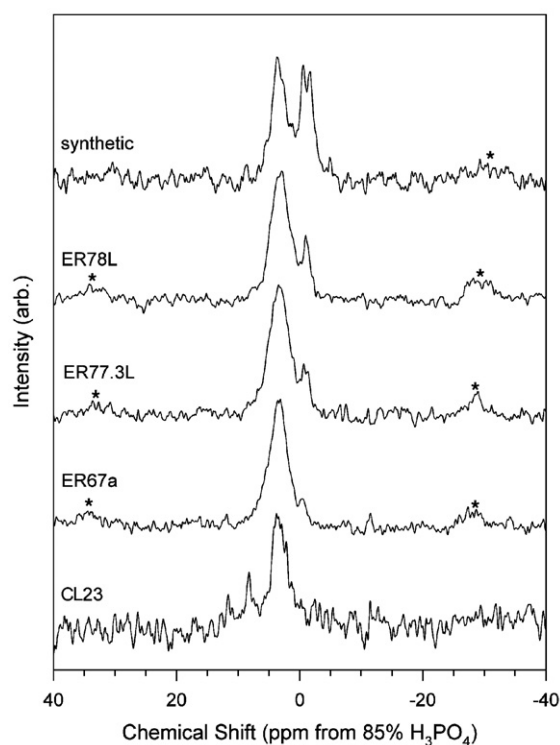


Fig. 3.  $^{31}\text{P}\{^1\text{H}\}$ CP/MAS NMR spectra of speleothem and synthetic samples studied (see text for description). Spectra were collected at a spin rate of 5 kHz and 1 s relaxation delay, with contact time of 5 ms for CL23 and 2 ms for ER67a, ER77.3L, ER78L and synthetic calcite/phosphate coprecipitate. Spectra represent (from bottom to top) 165,112, 139,094, 155,135, 100,000, and 100,000 acquisitions. Asterisks denote spinning sidebands.

Table 1

Peak positions and widths for  $^{31}\text{P}$  single-pulse (SP) and  $^{31}\text{P}\{^1\text{H}\}$ CP/MAS (CP) NMR spectra collected for the speleothem and synthetic samples

Sample	Experiment	$\delta_{\text{P-31}}$ (ppm)	FWHM (ppm)	Relative peak intensity (%)	Assignment
Synthetic	SP	3.4 <sup>1</sup>	3.0 <sup>1</sup>	47(5)	Calcite
		3.0	0.6	35(3)	Incl.
		-0.9	1.1	17(2)	Monetite
	CP	3.4	3.0		Calcite
		-0.5	1.4		Monetite
		-1.8	1.6		Monetite
ER78L	SP	3.2 <sup>1</sup>	3.6 <sup>1</sup>	26(5)	Calcite
		2.8	0.8	57(3)	Incl.
		-1.0	1.7	16(2)	Monetite
	CP	3.2	3.6		Calcite
		-1.1	1.4		Monetite
		3.3 <sup>1</sup>	3.9 <sup>1</sup>	30(6)	Calcite
ER77.3L	SP	2.9	0.6	62(3)	Incl.
		-1.0	1.1	8(2)	Monetite
		3.3	3.9		Calcite
	CP	-1.0	1.5		Monetite
		3.9 <sup>1</sup>	3.6 <sup>1</sup>	25(6)	Calcite
		2.9	0.9	71(4)	Incl.
ER67a	SP	-0.9	0.9	4(3)	Monetite
		3.9	3.6		Calcite
		-0.9	0.9		Monetite
	CP	3.2	5.6	100	Calcite
		3.6	2.9		Calcite

Relative peak intensities correspond to integrated peak areas from least-square fits of spectra obtained under quantitative conditions and are proportional to the relative concentration of P. Values in parentheses correspond to estimated uncertainty in the last digit. "Incl." indicates unidentified crystalline inclusion.

<sup>1</sup>Values constrained to equal those observed for the CP spectra.

$\delta_{\text{P-31}} = -0.5$  ppm (1.3 ppm FWHM) and  $-1.8$  ppm (1.5 ppm FWHM) that closely resemble those previously reported for monetite [42,43]. The presence of monetite is also supported by the occurrence of a small characteristic peak in the  $^1\text{H}$  SP MAS NMR spectra of these samples (see below).

The  $^{31}\text{P}$  SP spectra of the Grotta di Ernesto and synthetic samples also show a prominent narrow peak at a chemical shift  $\delta_{\text{P-31}} = 2.9$  ppm (0.7 to 0.9 ppm FWHM) that dominates the spectra, but which is notably absent from the CP spectra (cf. Figs. 1 and 3). The position and width of this narrow peak is within the range of those previously reported for hydroxylapatite [42–44], but is slightly shifted from our measurement for reagent grade material ( $\delta_{\text{P-31}} = 2.65$  ppm). Under our experimental conditions even a small fraction of hydroxylapatite would yield a peak in the CP spectra, because of its high  $^{31}\text{P}\{^1\text{H}\}$  CP efficiency [45]. Additional CP spectra were taken over a range of experimental conditions, particularly at short and long contact times (0.5 to 7 ms) and

long and short relaxation delays (up to 60 s), but no corresponding peak at  $\delta_{\text{P-31}} = 2.9$  ppm was observed. The narrow line shape (0.7 to 0.9 ppm FWHM) of this peak indicates a very uniform P environment and suggests strongly that it arises from a well-ordered crystalline phase. However, the  $^{31}\text{P}$  NMR properties of other possible Ca-phosphate phases such as tricalcium phosphate, whitlockite, and tetracalcium phosphate do not match any of our data [43,46,47]. We tentatively assign this peak at 2.9 ppm to an anhydrous Ca-orthophosphate but cannot identify the phase from the current data. Orthophosphate is indicated by the absence of spinning sidebands, which would be prominent for pyrophosphate groups [48]. Assignment to a Ca-phosphate seems likely because this peak also occurs in the synthetic sample, which was precipitated from a solution containing only  $\text{Na}^+$ ,  $\text{K}^+$ , and  $\text{Ca}^{2+}$  cations.

To obtain quantitative ratios for the three types of phosphate environments we fit the SP spectra taken under quantitative conditions (500 s relaxation delay) to a sum of Gaussian curves (Fig. 2), with the constraint that for each sample the width and position of the broad peak centered near  $\delta_{\text{P-31}} = 3.5$  ppm equal those observed in the corresponding CP spectrum. The results for the Grotta di Ernesto samples (Table 1) indicate that the majority of the P species present (57 to 71%) is represented by the peak at  $\delta_{\text{P-31}} = 2.9$  ppm, followed by 25 to 30% as phosphate coprecipitated in calcite (peak at  $\delta_{\text{P-31}} = 3.5$  ppm), and 4 to 16% as monetite (peak at  $\delta_{\text{P-31}} = -0.9$  ppm). The synthetic calcite/phosphate coprecipitate shows the same P species, but with the peak for phosphate in calcite the most abundant (47%) followed by the peak at  $\delta_{\text{P-31}} = 3.0$  ppm (35%) and monetite (17%). This result indicates that the synthesis method employed can reproduce the P species present in the natural samples.

Further support for the presence of monetite inclusions is provided by  $^1\text{H}$  SP MAS NMR data. For the Grotta di Ernesto samples the  $^1\text{H}$  spectra (Fig. 4) are dominated by a narrow peak at  $\delta_{\text{H-1}} = 4.8$  ppm, but also contain peaks at  $\delta_{\text{H-1}} = 1.5$  ppm and 13.9 ppm in addition to a shoulder on the main peak at about 7.4 ppm and a broad unresolved peak underlying all the peaks, centered at about 6.5 ppm. The dominant peak at  $\delta_{\text{H-1}} = 4.8$  ppm arises from aqueous fluid inclusions [49] whereas that at 1.5 ppm has been assigned to hydroxyl groups at defect sites in calcite [50]. The peak at  $\delta_{\text{H-1}} = 7.4$  ppm is characteristic of bicarbonate defects within the calcite structure [51] and the broad underlying peak, which is not evident at the scaling used for Fig. 4, likely arises from rigidly bound structural water [50]. The peak at  $\delta_{\text{H-1}} = 13.9$  ppm peak occurs in all the Grotta di

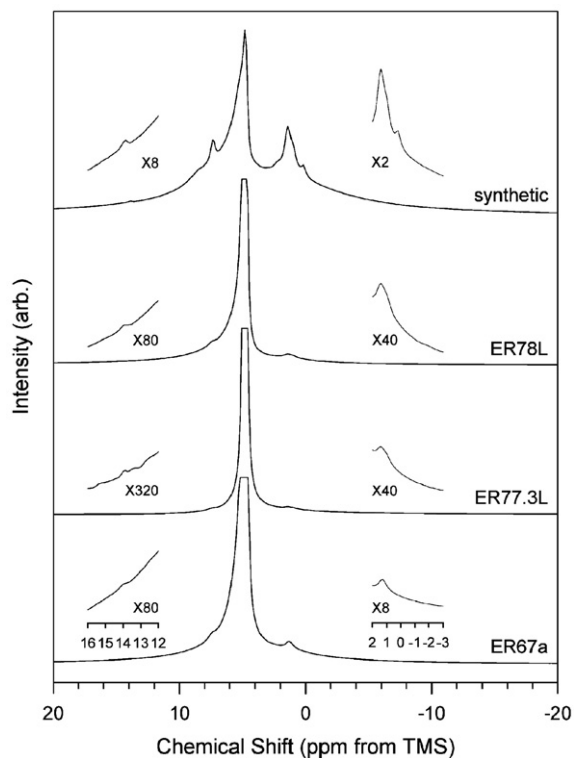


Fig. 4.  $^1\text{H}$  MAS NMR spectra of calcite speleothems and synthetic calcite/phosphate coprecipitate. Insets shown at expanded vertical scale to show the regions 16 to 12 ppm and 2 to  $-3$  ppm. Each spectrum was collected with a relaxation delay of 10 s for 6000 to 9000 acquisitions.

Ernesto and synthetic samples and is consistent with assignment to acidic protons in monetite [52]. This result supports the assignment of the  $^{31}\text{P}$  NMR peaks to this phase. Sample CL23 does not give a  $^1\text{H}$  NMR peak at 13.9 ppm, in agreement with the absence of peaks for monetite in the  $^{31}\text{P}$  spectra of this sample.

These  $^1\text{H}$  NMR spectra also provide further evidence for the absence of hydroxylapatite in the speleothem samples. Hydroxylapatite gives a narrow  $^1\text{H}$  NMR peak at  $\delta_{\text{H-1}}=0.2$  ppm [52], but a peak near this position was not observed for any of the natural samples (Fig. 4). Although the main  $^{31}\text{P}$  NMR peak for the Grotta di Ernesto samples occurs near the chemical shift for hydroxylapatite, the absence of a  $^1\text{H}$  NMR peak at  $\delta_{\text{H-1}}=0.2$  ppm for these samples provides strong evidence against assignment to this phase, especially considering that a  $^1\text{H}$  NMR peak for the less abundant monetite is observed. The synthetic calcite/phosphate coprecipitate does show a peak at  $\delta_{\text{H-1}}=0.2$  ppm (Fig. 4). However, this peak was also observed in the  $^1\text{H}$  MAS NMR spectra of calcite precipitated by the same method and seeds but in the absence of phosphate [51], and in

samples prepared in  $\text{D}_2\text{O}$  [53], suggesting that it arises from an impurity in the calcite seed crystals.

These observations indicate that the principal P species in the Grotta di Ernesto and synthetic samples, corresponding to the peak at  $\delta_{\text{P-31}}=2.9$  ppm, does not arise from hydroxylapatite. However, assignment to a crystalline phosphate inclusion, possibly originating as a surface precipitate, remains the most likely explanation for this NMR signal. Although we cannot completely rule out the possibility of a second type of phosphate environment in calcite at this time, assignment of the peak at  $\delta_{\text{P-31}}=2.9$  ppm to a calcite defect is very unlikely considering the small width of this peak (0.7 ppm FWHM), which reflects a very uniform bonding environment for phosphate as expected for a crystalline phase. This peak is narrower than those for many crystalline phosphates [42–44,46,47]. Phosphate defects in calcite are expected to exhibit a range of local structural environments for accommodating the size and charge difference between carbonate and phosphate groups, giving a distribution of  $^{31}\text{P}$  chemical shifts such as that observed for the peak near  $\delta_{\text{P-31}}=3.5$  ppm for all samples. The width of this peak (3–4 ppm, FWHM) spans the range of  $^{31}\text{P}$  chemical shifts for Ca-orthophosphates and is similar to that observed for amorphous calcium phosphate [54]. If a second, well-ordered type of phosphate environment could occur in calcite, it should be present in all samples. However, the peak at  $\delta_{\text{P-31}}=2.9$  ppm is completely absent in the spectra for the CL23 sample, but would have been detected even if it represented a small fraction of the P.

The low signal intensity observed in the  $^{31}\text{P}$  NMR spectra from the Grotte de Clamouse sample (CL23) indicates that this sample has the lowest P-content of the samples studied, consistent with the P concentrations measured for other samples from this locality (ca. 20 ppm [34]). The  $^{31}\text{P}$  NMR spectra of CL23 contain only the broad peak near  $\delta_{\text{P-31}}=3.5$  ppm (Figs. 1 and 3) and indicate that P is present only as individual phosphate ions incorporated into the calcite. Comparison of the absolute intensity of this peak to the corresponding resonance from the Grotta di Ernesto samples indicates that the concentration of P represented by this peak is comparable among all the samples. The lack of resonances from crystalline phases in the CL23 sample suggests that there is a P threshold for formation of surface precipitates, and, conversely, a limit for phosphate coprecipitation into the calcite structure.

With the information from the present study we can begin to understand the underlying mechanisms that control the incorporation of P in speleothems. Our results indicate that some P occurs in speleothems as

individual phosphate ions in calcite defects as suggested by Huang et al. [4]. This appears to be the only incorporation mechanism for the P-poor, defect-poor Grotte de Clamouse calcite. At higher P concentrations, phosphate defects in calcite also occur, but most of the P is incorporated as crystalline phosphate phases. At similar P concentrations, other factors such as crystal morphology, P speciation in the parent waters, and crystal growth rate might contribute to the differences observed in these samples. For example, differences in P distribution between the Grotta di Ernesto and synthetic samples, which have similar total P concentrations, might be related to the faster growth rate for the lab-grown crystals.

Even though there appears to be a limit for phosphate incorporation in the calcite structure, our study suggests that P remains a good indicator of environmental changes, provided the system is well-characterized. The residence time of water in the aquifer above the Grotta di Ernesto, which has been reported to be <1 week during major infiltration events [4], allows some P to be flushed before it can be mineralized in the soil. The periods between infiltration events are likely too long to prevent mineralization of P in soils. Since we observe the formation of precipitates over the course of a few hours in the seeded growth experiments and that adsorption of phosphate on the calcite surface has been reported to occur on the order of a few minutes [16] it is likely that these same processes may form surface precipitates in the span of a few days after a major infiltration event in a natural setting. In the time between infiltration events these surfaces would then be exposed to solutions with lower P concentrations and calcite precipitation would continue, enclosing any surface precipitates. These processes would then repeat over a given season giving a band concentrated in P with respect to the surrounding calcite matrix. The large spot size for SIMS and ELA-ICPMS (10–25  $\mu\text{m}$ ) relative to typical surface precipitate size (e.g., 3 nm height reported in Ref. [55]) and scanning geometry relative to the calcite growth surfaces will only give the average concentration for the area being scanned and not the concentration represented by crystalline surface precipitates and thus will likely prevent analyzed P concentrations from exceeding ca. 100–200 ppm.

The results of the present study have potentially wide ranging implications for the distribution of P in other low-temperature geochemical settings dominated by carbonates. Interactions of dissolved inorganic phosphate with the surface of calcite and corresponding incorporation mechanisms similar to those we observe in the synthetic and speleothem samples can be expected

to occur also in soils and sediments, affecting the distribution and cycling of P in these environments. Incorporation of phosphate in calcite as crystalline inclusions is likely to reduce P mobility in sediments during recrystallization and delay formation of the thermodynamically stable apatite phases. Current models cannot predict surface precipitation and, indeed, distinguishing whether phosphate removal from solution occurs by sorption, coprecipitation, or formation of a surface precipitate is a difficult problem [56]. Clearly, standard treatments for trace element incorporation, such as linear distribution coefficients, are insufficient to describe the phosphate distribution we observe in the speleothem and synthetic samples, especially at higher P concentration. Further analytical and experimental work is needed to identify the main phosphate inclusion we observe in the calcite speleothems, to determine whether similar P distributions occur in carbonate minerals from other low-temperature environments, and how this distribution depends on the precipitation conditions and growth rate. However, our results show that solid-state  $^{31}\text{P}$  NMR spectroscopy can be used to determine *in situ* the distribution of P in carbonate minerals at the concentrations found in nature.

#### 4. Conclusions

Our results indicate that calcite speleothems can contain phosphate in several forms, including phosphate defects in calcite and several types of coexisting crystalline phosphate inclusions. The presence of crystalline inclusions indicates that the ability of calcite speleothems to record P flushing events is not limited by the solubility of phosphate ions in the calcite structure. Calcite crystal growth appears capable of effectively encasing surface precipitates that form during periods of high P flux, forming inclusions. The results for the CL23 sample, however, indicate that these precipitates do not form in all cases and that their formation is likely related to periods of higher P influx. The phosphate/calcite coprecipitation experiment indicates that it is possible to reproduce in chemically simple systems the essential P environments present in the speleothems, suggesting that the formation of the included phases does not depend on other cations or anions present at trace concentration.

#### Acknowledgments

We thank Ian Fairchild and two anonymous reviewers for the insightful comments that led to many improvements to the manuscript. This work

was supported by the US-NSF through the Center for Environmental Molecular Science (CHE-0221934) and EAR-0310200 (B.L.P). S.F. acknowledges support from the AQUAPAST project (funded by Provincia Autonoma di Trento) and FG 668 of DFG (DAPHNE).

## References

- [1] J.U.L. Baldini, F. McDermott, I.J. Fairchild, Structure of the 8200-year cold event revealed by a speleothem trace element record, *Science* 296 (2002) 2203–2206.
- [2] M.S. Roberts, P.L. Smart, A. Baker, Annual trace element variations in a Holocene speleothem, *Earth Planet. Sci. Lett.* 154 (1998) 237–246.
- [3] I.J. Fairchild, A. Baker, A. Borsato, S. Frisia, R.W. Hinton, F. McDermott, A.F. Tooth, Annual to sub-annual resolution of multiple trace-element trends in speleothems, *J. Geol. Soc. (Lond.)* 158 (2001) 831–841.
- [4] H.M. Huang, I.J. Fairchild, A. Borsato, S. Frisia, N.J. Cassidy, F. McDermott, C.J. Hawkesworth, Seasonal variations in Sr, Mg and P in modern speleothems (Grotta di Ernesto, Italy), *Chem. Geol.* 175 (2001) 429–448.
- [5] A.A. Finch, P.A. Shaw, G.P. Weedon, K. Holmgren, Trace element variation in speleothem aragonite: potential for palaeoenvironmental reconstruction, *Earth Planet. Sci. Lett.* 186 (2001) 255–267.
- [6] P.C. Treble, J. Chappell, J.M.G. Shelley, Complex speleothem growth processes revealed by trace element mapping and scanning electron microscopy of annual layers, *Geochim. Cosmochim. Acta* 69 (2005) 4855–4863.
- [7] J.M. Desmarchelier, J.C. Hellstrom, M.T. McCulloch, Rapid trace element analysis of speleothems by ELA-ICP-MS, *Chem. Geol.* 231 (2006) 102–117.
- [8] A. Baker, P.L. Smart, R.L. Edwards, D.A. Richards, Annual growth banding in a cave stalagmite, *Nature* 364 (1993) 518–520.
- [9] S. Frisia, A. Borsato, I.J. Fairchild, J. Susini, Variations in atmospheric sulphate recorded in stalagmites by synchrotron micro-XRF and XANES analyses, *Earth Planet. Sci. Lett.* 235 (2005) 729–740.
- [10] I.J. Fairchild, C.L. Smith, A. Baker, L. Fuller, C. Spotl, D. Mathey, F. McDermott, E.I.M.F., Modification and preservation of environmental signals in speleothems, *Earth-Sci. Rev.* 75 (2006) 105–153.
- [11] S. Frisia, A. Borsato, I.J. Fairchild, F. McDermott, Calcite fabrics, growth mechanisms, and environments of formation in speleothems from the Italian Alps and southwestern Ireland, *J. Sediment. Res.* 70 (2000) 1183–1196.
- [12] R.A. Griffin, J.J. Jurinak, Interaction of phosphate with calcite, *Soil Sci. Soc. Am. J.* 37 (1973) 847–850.
- [13] M.M. Reddy, Crystallization of calcium carbonate in presence of trace concentrations of phosphorus containing anions. 1. Inhibition by phosphate and glycerophosphate ions at pH 8.8 and 25 °C, *J. Cryst. Growth* 41 (1977) 287–295.
- [14] J. Dekanel, J.W. Morse, Chemistry of orthophosphate uptake from seawater onto calcite and aragonite, *Geochim. Cosmochim. Acta* 42 (1978) 1335–1340.
- [15] H.J. Meyer, The influence of impurities on the growth rate of calcite, *J. Cryst. Growth* 66 (1984) 639–646.
- [16] W.A. House, L. Donaldson, Adsorption and coprecipitation of phosphate on calcite, *J. Colloid Interface Sci.* 112 (1986) 309–324.
- [17] W.A. House, Inhibition of calcite crystal growth by inorganic phosphate, *J. Colloid Interface Sci.* 119 (1987) 505–511.
- [18] A. Mucci, Growth kinetics and composition of magnesian calcite overgrowths precipitated from seawater: quantitative influence of orthophosphate ions, *Geochim. Cosmochim. Acta* 50 (1986) 2255–2265.
- [19] E.A. Burton, L.M. Walter, The role of pH in phosphate inhibition of calcite and aragonite precipitation rates in seawater, *Geochim. Cosmochim. Acta* 54 (1990) 797–808.
- [20] L.J. Plant, W.A. House, Precipitation of calcite in the presence of inorganic phosphate, *Colloids Surf., A Physicochem. Eng. Asp.* 203 (2002) 143–153.
- [21] Z.R. Hinedi, S. Goldberg, A.C. Chang, J.P. Yesinowski, A <sup>31</sup>P and <sup>1</sup>H MAS NMR study of phosphate sorption onto calcium carbonate, *J. Colloid Interface Sci.* 152 (1992) 141–160.
- [22] P.M. Dove, M.F. Hochella, Calcite precipitation mechanisms and inhibition by orthophosphate: in situ observations by scanning force microscopy, *Geochim. Cosmochim. Acta* 57 (1993) 705–714.
- [23] P. Montagna, M. McCulloch, M. Taviani, C. Mazzoli, B. Vendrell, Phosphorus in cold-water corals as a proxy for seawater nutrient chemistry, *Science* 312 (2006) 1788–1791.
- [24] R. Lookman, H. Geerts, P. Grobet, R. Merckx, K. Vlassak, Phosphate speciation in excessively fertilized soil: a <sup>31</sup>P and <sup>27</sup>Al MAS NMR spectroscopy study, *Eur. J. Soil Sci.* 47 (1996) 125–130.
- [25] L.L. Clark, E.D. Ingall, R. Benner, Marine phosphorus is selectively remineralized, *Nature* 393 (1998) 426–426.
- [26] L.C. Kolowith, R.A. Berner, Weathering of phosphorus in black shales, *Glob. Biogeochem. Cycles* 16 (2002).
- [27] S. Hunger, H. Cho, J.T. Sims, D.L. Sparks, Direct speciation of phosphorus in alum-amended poultry litter: solid-state <sup>31</sup>P NMR investigation, *Environ. Sci. Technol.* 38 (2004) 674–681.
- [28] A. Kuczumow, D. Genty, P. Chevallier, J. Nowak, M. Florek, A. Buczynska, X-ray and electron microprobe investigation of the speleothems from Godarville tunnel, *X-ray Spectrom.* 34 (2005) 502–508.
- [29] F. McDermott, S. Frisia, Y.M. Huang, A. Longinelli, B. Spiro, T.H.E. Heaton, C.J. Hawkesworth, A. Borsato, E. Keppens, I.J. Fairchild, K. van der Borg, S. Verheyden, E. Selmo, Holocene climate variability in Europe: evidence from  $\delta^{18}\text{O}$ , textural and extension-rate variations in three speleothems, *Quat. Sci. Rev.* 18 (1999) 1021–1038.
- [30] S. Frisia, A. Borsato, I.J. Fairchild, F. McDermott, E.M. Selmo, Aragonite–calcite relationships in speleothems (Grotte de Clamouse, France): environment, fabrics, and carbonate geochemistry, *J. Sediment. Res.* 72 (2002) 687–699.
- [31] V. Plagnes, C. Causse, D. Genty, M. Paterne, D. Blamart, A discontinuous climatic record from 187 to 74 ka from a speleothem of the Clamouse Cave (south of France), *Earth Planet. Sci. Lett.* 201 (2002) 87–103.
- [32] E.A. McMillan, I.J. Fairchild, S. Frisia, A. Borsato, F. McDermott, Annual trace element cycles in calcite–aragonite speleothems: evidence of drought in the western Mediterranean 1200–1100 yr BP, *J. Quat. Sci.* 20 (2005) 423–433.
- [33] S. Frisia, A. Borsato, N. Preto, F. McDermott, Late Holocene annual growth in three Alpine stalagmites records the influence of solar activity and the North Atlantic Oscillation on winter climate, *Earth Planet. Sci. Lett.* 216 (2003) 411–424.

- [34] E.A. McMillan, Tests for paleoaridity in Holocene Stalagmites from SW Europe. Ph.D. Thesis (unpublished), Keele University, U.K., (2006).
- [35] S.J. Zhong, A. Mucci, Calcite precipitation in seawater using a constant addition technique: a new overall reaction kinetic expression, *Geochim. Cosmochim. Acta* 57 (1993) 1409–1417.
- [36] A.J. Tesoriero, J.F. Pankow, Solid solution partitioning of  $\text{Sr}^{2+}$ ,  $\text{Ba}^{2+}$ , and  $\text{Cd}^{2+}$  to calcite, *Geochim. Cosmochim. Acta* 60 (1996) 1053–1063.
- [37] R.J. Reeder, M. Nugent, G.M. Lamble, C.D. Tait, D.E. Morris, Uranyl incorporation into calcite and aragonite: XAFS and luminescence studies, *Environ. Sci. Technol.* 34 (2000) 638–644.
- [38] D.L. Parkhurst, C.A.J. Appelo, User's guide to PHREEQC (Version 2) — a computer program for speciation, batch-reaction, one-dimensional transport, and inverse geochemical calculations, U. S. Geol. Surv. Water Res. Inv. Rept., 1999, pp. 99–4259.
- [39] P.O. Hall, R.C. Aller, Rapid, small-volume, flow injection analysis for  $\Sigma\text{CO}_2$  and  $\text{NH}_4^+$  in marine and fresh waters, *Limnol. Oceanogr.* 37 (1992) 1113–1119.
- [40] M.A. Nanny, R.A. Minear, J.A.e. Lenheer, Nuclear Magnetic Resonance Spectroscopy in Environmental Science and Technology, Oxford University Press, London, 1997.
- [41] F. McDermott, H.P. Schwarcz, P.J. Rowe, Isotopes in speleothems. In: *Isotopes in Palaeoenvironmental Research*, Springer, Dordrecht, The Netherlands, (in press).
- [42] W.P. Aue, A.H. Roufousse, M.J. Glimcher, R.G. Griffin, Solid-state  $^{31}\text{P}$  nuclear magnetic resonance studies of synthetic solid phases of calcium phosphate: potential models of bone mineral, *Biochemistry* 23 (1984) 6110–6114.
- [43] P.S. Belton, R.K. Harris, P.J. Wilkes, Solid-state  $^{31}\text{P}$  NMR studies of synthetic inorganic calcium phosphates, *J. Phys. Chem. Solids* 49 (1988) 21–27.
- [44] W.P. Rothwell, J.S. Waugh, J.P. Yesinowski, High-resolution variable temperature  $^{31}\text{P}$  NMR of solid calcium phosphates, *J. Am. Chem. Soc.* 102 (1980) 2637–2643.
- [45] A. Kafak, D. Chmielewski, A. Gorecki, A. Slorarczyk, W. Kolodziejcki, Efficiency of  $^1\text{H}\rightarrow^{31}\text{P}$  cross-polarization in bone apatite and its mineral standards, *Solid State Nucl. Magn. Reson.* 29 (2006) 345–348.
- [46] J. Vogel, C. Russel, G. Gunther, P. Hartmann, F. Vizethum, N. Bergner, Characterization of plasma-sprayed hydroxyapatite by  $^{31}\text{P}$ -MAS-NMR and the effect of subsequent annealing, *J. Mater. Sci., Mater. Med.* 7 (1996) 495–499.
- [47] M. Bohner, J. Lemaitre, A.P. Legrand, J.B.D. de la Caillerie, P. Belgrand, Synthesis, X-ray diffraction and solid-state  $^{31}\text{P}$  magic angle spinning NMR study of  $\alpha$ -tricalcium orthophosphate, *J. Mater. Sci., Mater. Med.* 7 (1996) 457–463.
- [48] D. Prochnow, A.R. Grimmer, D. Freude, Solid-state NMR studies of  $^{17}\text{O}$ -enriched pyrophosphates, *Solid State Nucl. Magn. Reson.* 30 (2006) 69–74.
- [49] J.P. Yesinowski, H. Eckert, G.R. Rossman, Characterization of hydrous species in minerals by high-speed  $^1\text{H}$  MAS-NMR, *J. Am. Chem. Soc.* 110 (1988) 1367–1375.
- [50] S.J. Gaffey,  $\text{H}_2\text{O}$  and  $\text{OH}$  in echinoid calcite: a spectroscopic study, *Am. Mineral.* 80 (1995) 947–959.
- [51] J. Feng, Y. Lee, R.J. Reeder, B.L. Phillips, Observation of bicarbonate in calcite by NMR spectroscopy, *Am. Mineral.* 91 (2006) 957–960.
- [52] J.P. Yesinowski, H. Eckert, Hydrogen environments in calcium phosphates:  $^1\text{H}$  MAS NMR at high spinning speeds, *J. Am. Chem. Soc.* 109 (1987) 6274–6282.
- [53] B.L. Phillips, Y.J. Lee, R.J. Reeder, Organic coprecipitates with calcite: NMR spectroscopic evidence, *Environ. Sci. Technol.* 39 (2005) 4533–4539.
- [54] J. Tropp, N.C. Blumenthal, J.S. Waugh, Phosphorus NMR study of solid amorphous calcium phosphate, *J. Am. Chem. Soc.* 105 (1983) 22–26.
- [55] V.G.R. Chada, D.B. Hausner, D.R. Strongin, A.A. Rouff, R.J. Reeder, Divalent Cd and Pb uptake on calcite  $\{10\bar{1}4\}$  cleavage faces: an XPS and AFM study, *J. Colloid Interface Sci.* 288 (2005) 350–360.
- [56] L. Li, R. Stanforth, Distinguishing adsorption and surface precipitation of phosphate on goethite ( $\alpha\text{-FeOOH}$ ), *J. Colloid Interface Sci.* 230 (2000) 12–21.